Green luminescence of InGaN nanowires grown on silicon substrates by molecular beam epitaxy

Kevin D. Goodman,[a] Vladimir V. Protasenko,[a] Jai Verma, Thomas H. Kosel, Huili G. Xing, and Debdeep Jena
Department of Electrical Engineering, 131 Stinson-Remick Hall, University of Notre Dame, Notre Dame, Indiana 46556, USA

(Received 10 August 2010; accepted 22 February 2011; published online 22 April 2011)

Indium gallium nitride nanowires show promise as being prime candidates for optical devices since they can be grown with band gaps spanning the visible spectra, while at the same time can be composed of stress free material. The goal of the work presented here was to obtain InGaN nanowires producing green emission at room temperature. Two growth recipes were found to yield InGaN nanowire growth on silicon substrates using plasma-assisted molecular beam epitaxy. At room temperature the photoluminescence (PL) of wire ensembles indeed peaked at 530 nm but, in addition, it was discovered that at low temperatures the emission often covered a broader (360–700 nm) spectrum. This broad optical range indicated indium content fluctuations in individual wires, wire-to-wire fluctuations, or a combination of the two. EDX measurements performed on single wires confirmed this hypothesis and correlated well with PL data. Low temperature PL studies of InGaN *individual* wires also revealed interwire and intrawire inhomogeneity of emission spectra stemming from a nonuniform indium distribution. The emission quantum yield for bright single wires was extracted to be more than 50% at 4 K. The findings suggest that the wire surfaces do not efficiently quench optical emission at low temperatures. These defect-free wires offer not only a potential path for green emitters, but also as integrated phosphors for broad spectral emission. © *2011 American Institute of Physics*. [doi:10.1063/1.3575323]

I. INTRODUCTION

Nitride nanowires are a compelling research topic due to their wide span of energy band gaps and low dislocation content. In particular, the InGaN semiconductor material system is capable of producing emission at red, blue, and green wavelengths. These three colors can be suitably combined to create white light sources with high rendering value. Such sources are desirable for reduction of energy spent in lighting, which is a large fraction of the world energy consumption.[1]

Of the three colors needed for such a device, high efficiency red and blue LEDs have been successfully demonstrated in different semiconductor systems. LEDs emitting in the green region of the spectrum with high efficiencies, however, have been problematic. The reason for the drop in efficiency near these wavelengths is the lattice mismatch between high indium composition InGaN and the common GaN substrates. Due to the high level of strain and associated defects, such InGaN layers often contain nonradiative recombination sites lowering the radiative efficiency. LEDs emitting in the green spectrum currently have attained a record 40% internal efficiency.[2] Although it is an incredible statistic, it also indicates that there is still need for improvement. Nanowires offer a method of growing material with a high indium content free of strain related defects on a wider choice of substrates.[3]

Using chemical vapor deposition (CVD) growth methods, several groups have produced a complete compositional range of $In_xGa_{1-x}N$ nanowire materials, spanning the energy gap from InN (0.7 eV, emission wavelength $\lambda = 1.7$ μm) to GaN (3.4 eV, $\lambda = 365$ nm).[4] Also, there have been numerous reports on molecular beam epitaxy (MBE) growth of pure binary GaN and InN wires, or InGaN quantum wells incorporated in GaN wires.[5–13] To date, however, there have been only a few reports on the MBE growth of ternary InGaN nanowires (see Refs. 7, 14 for examples). In this work, the MBE growth and characterization of InGaN wires with high indium compositions is reported.

Unlike most CVD growth techniques, the nanowires discussed in the article are grown without foreign metal catalysts removing any threat of introducing mid gap states which promote nonradiative recombination of carriers. Reports have shown that nanowires grown using metal catalysts lead to incorporation of catalyst atoms in the body of the nanowire.[15] These atoms typically introduce deep level traps in the bandgap and act as nonradiative recombination sites. Self-catalyzed MBE wires remove this bottleneck for efficient light emission.

Scanning electron microscopy (SEM) and transmission electron microscopy (TEM) demonstrated good crystal quality of the MBE grown InGaN wires with no defects observed. All InGaN nanowire ensembles yielded green emission at room temperature, but for some wire ensembles a bluish emission spanning from the GaN peak at ~360–500 nm became prominent at low temperatures. Energy dispersive x-ray analysis (EDX) studies revealed that the indium

[a]Authors to whom correspondence should be addressed. Electronic mail: kgoodman@nd.edu and vprotase@nd.edu.

Downloaded 14 May 2011 to 129.74.159.82. Redistribution subject to AIP license or copyright; see http://jap.aip.org/about/rights_and_permissions

concentration in the wires varies along their lengths despite unchanging growth conditions. This unintentional grading of the InGaN nanowire bandgap can be useful for integrated broad spectrum emitters or phosphors.

II. MBE GROWTH OF InGaN WIRES

InGaN nanowires have been grown by plasma-assisted MBE using no foreign catalyst materials. Silicon (111) p-type substrates were dipped in 10% buffered HF for 90 s to remove the native oxide, mounted onto lapped silicon carrier wafers using molten indium as an adhesive, and loaded into a Veeco Gen 930 MBE system. Substrate temperatures noted herein were measured using a thermocouple. Once standard outgassing bakes at 200 °C for 7 h and 400 °C for 2 h were completed in preparation chambers, the samples were baked in the growth chamber at 750 °C for 15 min and 850 °C for 10 min to further remove native oxides.[5] Following growth, the samples were imaged using a Hitachi 4500 scanning electron microscope (SEM), FEI Helios Nanolab SEM, and a FEI Magellan 400 SEM. Transmission electron microscopy images were taken using a JEOL 2010 system using a 200 kV beam along with a FEI Titan microscope using a 300 kV bias.

Initial growth studies followed the method for nanowire growth reported by Kikuchi *et al*.[16] Using this technique, GaN nanowires were first grown for a short time to establish nanowire nucleation. Once GaN nanowires were established, growth conditions were altered to allow for the growth of InGaN nanowires. Gallium droplets were deposited onto silicon substrates at a growth temperature (T_{sub}) of 530 °C for 40 s using a gallium beam equivalent pressure (BEP) F_{Ga} $\sim$2x10^{-8} Torr. Upon deposition, the gallium cell was closed and the nitrogen cell opened for 1 min using a plasma power of 450 Ws and nitrogen pressure of 2×10^{-5} Torr at the same substrate temperature. Following the nitrogen plasma treatment, T_{sub} was ramped to 830 °C upon which GaN nanowires were grown for 30 min using $F_{Ga}$$\sim$$10^{-7}$ Torr. Following the GaN nanowire growth, T_{sub} was lowered to allow for incorporation of indium and InGaN was grown for 90 mins using $F_{Ga} \sim 2.3 \times 10^{-8}$ Torr and $F_{In} \sim 7.5 \times 10^{-8}$ Torr.

Growth kinetics and other observations during the formation of the GaN and InGaN nanowires are reported elsewhere.[17] As reported earlier by various groups,[7,18] a nitrogen rich growth environment combined with a higher substrate temperature than is used for most thin film growths favors the growth of GaN nanowires. The same general scheme applies for InGaN nanowires. The most dramatic change when switching from GaN to InGaN growth is the substrate temperature. The low vaporization temperature of indium does not allow for the high growth temperatures that are normally used in GaN nanowire growths. Since the substrate temperature plays one of the most important roles in formation of InGaN nanowires, the growth dependence on this variable will now be discussed.

Temperature dependent results of InGaN nanowire growths are summarized in Fig. 1, in which SEM top and side view images show the wire growth evolution. As can be

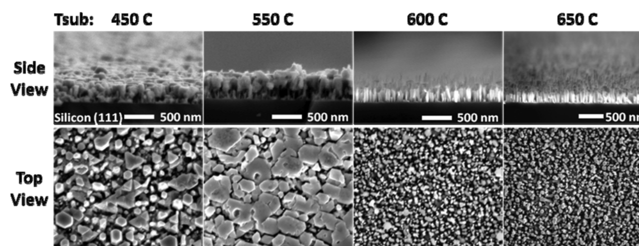

FIG. 1. Scanning electron microscopy images reveal lower growth temperatures result in clumps of material. Once T_{sub} reaches 650 °C, nanowire growth is accomplished. Note: scale bar is valid for both top and side views.

seen, below a growth temperature of 600 °C, the growths do not yield nanowire structures. Once T_{sub} reaches 600 °C, nanowire shapes start to appear, and finally at 650 °C, nanowire growth occurs. Examination of the data hints that at lower substrate temperatures the metal atoms do not diffuse toward the wire tip. Instead, at low temperatures, as shown in Fig. 1, growth occurs laterally as opposed to vertically, indicating that the metal atoms do not have a high enough diffusion coefficient to transverse the nanowire sidewalls. As the growth temperature reaches 600 °C, SEM images indicate a slight enhancement of the diffusion constant along the sidewalls as nanowires become more pronounced. However, at 600 °C, at the tips of the wires which would be slightly cooler than the base, growth switches from vertical to horizontal. Once the temperature is increased to 650 °C, this problem is overcome and nanowire growth is obtained. This is in line with a wire growth model that prescribes higher metal diffusion on the nanowire sidewalls as a primary driving force of the growth.[18]

Once the optimal T_{sub} was found yielding InGaN nanowire growth that exhibited desired optical emission, it was found that the GaN nanowire "seeding" on the silicon substrates was not necessary. At this point, growths were carried out in a much simpler manner. Growths occurred at a substrate temperature of 650 °C, using gallium BEP of $F_{Ga} \sim 2.3 \times 10^{-8}$ Torr, indium BEP of $F_{In} \sim 8 \times 10^{-8}$ Torr, a nitrogen plasma power of 450 W, and pressure of 2×10^{-5} Torr. There were no nucleation layers or promoter materials deposited before growth on silicon. Once the substrate was at the growth temperature (650 °C), all cells (In, Ga, N) were opened simultaneously and conditions were held constant until the end of the growth. Nanowires grown using this method are similar in size and shape as those grown using gallium seeds. There was seen, however, a difference between the densities yielded from the two growth methods. Concerning growths where gallium droplets were used, the nanowire density would increase with an increase of gallium metal initially deposited. However, nanowire density was also dependent on growth time. Longer growth times resulted in a higher nanowire density for the seeded growths regardless of the initial amount of gallium deposited. A note should be made, however, that the density dependence on the gallium droplets was only observed in GaN nanowires. The density dependence on seeding conditions was not investigated for InGaN nanowires.

Using the above growth conditions, nanowires were grown at a rate of $\sim$250 nm/h. Diameters ranged from 50 to

Downloaded 14 May 2011 to 129.74.159.82. Redistribution subject to AIP license or copyright; see http://jap.aip.org/about/rights_and_permissions

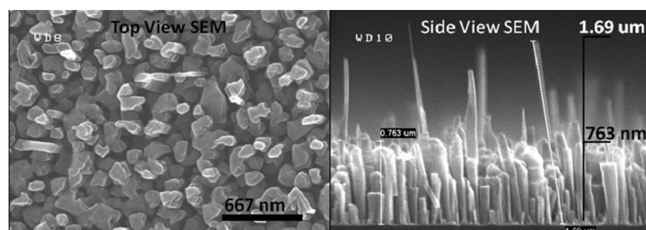

FIG. 2. Scanning electron microscopy images of InGaN nanowires. Left: top view. Right: side view of cleaved sample. Note two distinct wire shapes, short and thick compared to tall and thin.

100 nm, as seen in representative SEM images in Fig. 2. It is interesting to note that the wires are not always parallel to each other but angle slightly at a few degrees. Further, the InGaN nanowires grow yielding two distinct types: those which are short and thick in diameter and those that are tall and thin in diameter.

Observing the ratio between the two types of wires in SEM images, it is noted that roughly 1 out of 10 wires will be of the tall and thin nature. While this "two geometry" growth characteristic is seen in InGaN wires, both seeded and nonseeded, the same is not seen in growths of GaN nanowires; which are grown at 830 °C. This leaves two variables which could be the cause of the phenomenon; the lower substrate temperature used for InGaN growth or the inclusion of indium itself.

To separate the two possible variables, a GaN nanowire growth using a substrate temperature of 800 °C; a lower than usual temperature for GaN nanowires; was carried out in efforts to determine the cause of the two distinct shapes. SEM images of this GaN growth shown in Fig. 3 reveal that there are also two general heights of nanowires as was seen with the InGaN wires. This data is implying that the cause of the nonuniform nanowire height is due to the lower substrate temperature as opposed to the inclusion of indium. A hypothesis to explain this effect is that the lower substrate temperature does not give the metal atoms as much kinetic energy to more evenly distribute among the wires as the growth is occurring.

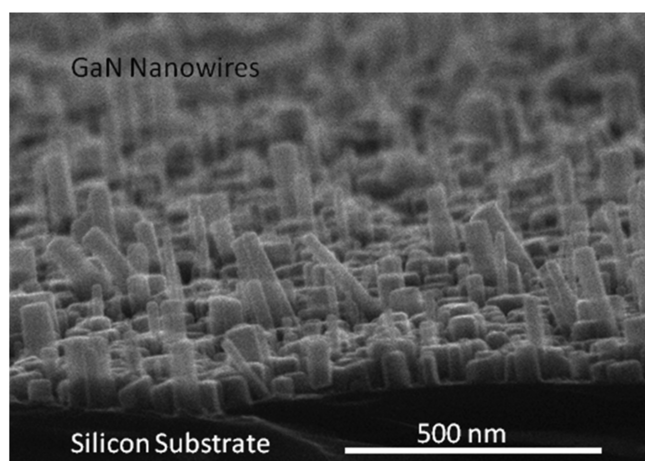

FIG. 3. Scanning electron microscope image of GaN nanowires grown at 800 °C. Note compared to the InGaN nanowires grown at the same temperature, these wires also grow in two distinct heights, while the diameters of the GaN nanowires do not show such segregation in value as the InGaN wires.

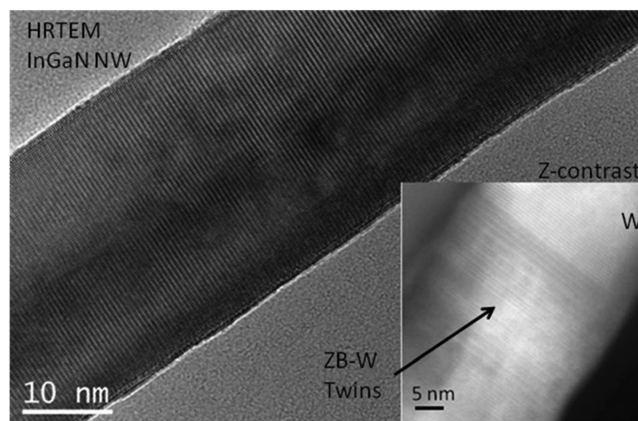

FIG. 4. High resolution transmission electron microscopy image of InGaN nanowire. Defect free lattice imaging of an InGaN nanowire is shown. Inset shows atomic contrast image displaying stacking faults between wurtzite and zinc blende materials.

Examining the diameters of the wires of this 800 °C GaN growth, they all seem to be relatively centered around 75 nm. This implies that the diameter variation is more likely due to the indium content of the wires. While this is an interesting occurrence, no quantitative answer to its origin has been seen in the results thus far. Qualitatively, concerning the two distinct diameter groupings shown to occur only in InGaN growths; this characteristic could be due to the different indium concentrations at the base of the wires dictating the diameter of the wires due to a dependence of free energy vs. diameter being heavily weighted by indium content.

High resolution TEM images of harvested InGaN nanowires are shown in Fig. 4 revealing high quality growth without threading dislocations as was the goal of the experiment. The inset shows the atomic contrast of a nanowire revealing the twinning in the stacking sequence switching between wurtzite and zinc blende material that was observed in a percentage of the population sampled.

To compare the optical properties of InGaN nanowires with InGaN thin films, ~200 nm thick InGaN films were grown on GaN-on-sapphire templates by MBE. Before growing the InGaN layer a 50 nm GaN buffer layer was used. The substrate temperature for growth of the GaN was 550 °C and then changed to 530 °C for growth of the InGaN layer. The RF power was kept at 350 W and the ratio of gallium to indium flux was ~0.8. AFM scans of the samples exhibited a ~2.8 nm rms roughness on 1x1 micron areas. X-ray diffraction (XRD) spectra of the films yielded an indium composition of ~21%.

III. OPTICAL EMISSION OF NANOWIRE ENSEMBLES

Photoluminescence (PL) studies were performed using a home-built setup which includes the following major "blocks": (a) a Liconix (Kimmon) HeCd laser (325 nm emission) for sample excitation, (b) an Acton 2500i spectrometer, (c) two CCD cameras for beam positioning, (d) a Janis CT-500 cryostat, and (e) miscellaneous optical elements (lenses,

Downloaded 14 May 2011 to 129.74.159.82. Redistribution subject to AIP license or copyright; see http://jap.aip.org/about/rights_and_permissions

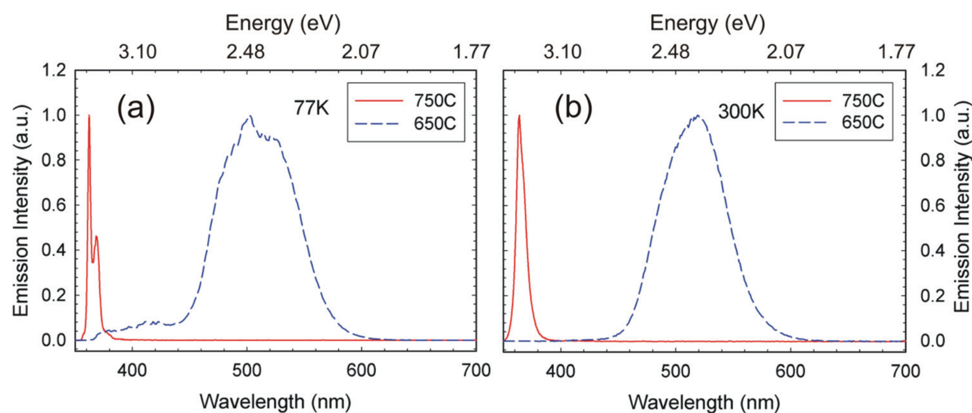

FIG. 5. (Color online) Normalized emission spectra of InGaN wires grown at 650 °C [blue (dashed) line] and 750 °C [red (solid) line] Si substrate temperature. Photoluminescence spectra was measured at 77 K (a) and 300 K (b) temperatures. Sample grown at 750 °C shows only a pure GaN peak as a result of no indium incorporation.

attenuation filters, dichroic beam splitter, barrier filters, and mirrors) for beam alignment and emission filtering.

Photoluminescence spectra of the InGaN wires were found to be very sensitive to the growth temperature. InGaN wires grown at elevated temperatures exhibit minor variations in their morphology compared to those grown at 650 °C. However, accompanying photoluminescence experiments clearly indicate compositional changes. For example, Fig. 5 shows normalized PL spectra of samples grown at 650 and 750 °C and measured at 77 and 300 K. The increase in T_{sub} has led to a complete disappearance of the green emission, which is an indication of indium evaporating from the surface at high temperatures. In contrast, 650 °C growth yields InGaN wires emit green light centered at 520 nm and no substantial ~360 nm GaN emission has been detected at room temperature as well as at 77 K.

To extract the effects of substrate temperature on indium content, samples were grown to investigate the substrate temperature window between 650 and 800 °C. Besides omitting the 750 and 850 °C outgas, growths were carried out in the same manner as the nanowires pictured in Fig. 1. Growths at 650 and 675 °C yielded material with PL peaks at 520 and 482.5 nm, equating to an indium concentration of 21 and 17%, respectively, when using a bowing coefficient of 2.6.[19] Growths at 725, 750, and 775 °C yielded PL peaks at 365–366 nm, which implies no indium content. Note that omitting the outgas step could allow for a native oxide on the silicon surface as opposed to growths in Fig. 1. Regardless, the data here shows that substrate temperature plays a vital role in the final indium content of the nanowires. While groups have found that higher substrate temperatures for MBE grown GaN nanowires yields less defect related luminescence,[20] the data here reveals that a high growth temperature is not permissible when growing InGaN nanowires.

For nonseeded growth, PL spectra of wires were compared with the spectra of the 200 nm thick InGaN films (Fig. 6). Note in the figure that there is a large GaN peak in the nanowire spectra. Details of the origin of the GaN material within the InGaN wires is discussed in the upcoming section regarding compositional studies. As the PL is indicating a pure GaN material within the nanowire, one could postulate that the higher wavelength emission from the nanowires is due to defects within the GaN. However, the high-resolution transmission electron microscopy image of Fig. 4 indicates defect free InGaN material. This combined with the EDX data in the upcoming compositional studies section suggest the green emission stems from InGaN incorporation rather than defects in the GaN material.

To select the data free of photobleaching, a few consecutive spectra scans are always performed to observe the spectral stability. It is obvious that the emission properties of nanowires and thin films are quite different: (a) the emission of the wires is broader and often includes a GaN peak, (b) the PL emission intensity of wires is ~3 orders of magnitude stronger than that of the film measured at 4 K and almost 5 orders stronger at room temperature, and (c) the emission intensity of wires decreases nearly 10 times when the temperature increases from 4 to 300 K; for the thin film, this factor is ~500. If it is assumed that the low temperature emission quantum yield (QY) is close to 100%, then based

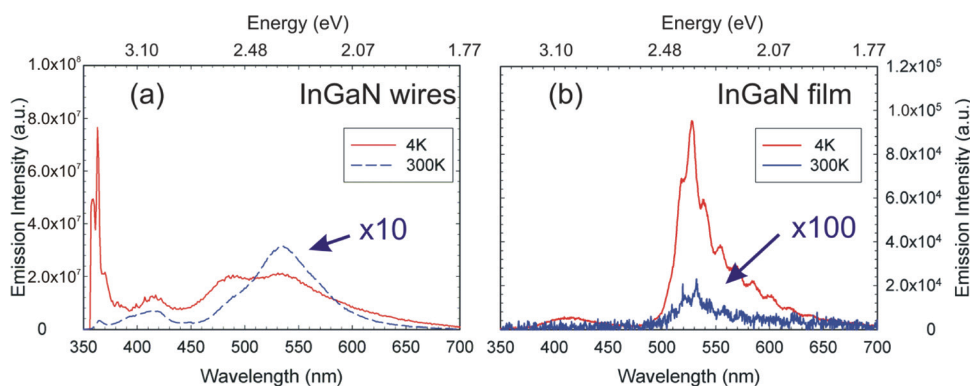

FIG. 6. (Color online) Emission spectra of InGaN wires (a) and film (b) measured at 300 K [blue (dashed) line] and 4 K [red (solid) line]. The emission intensity obtained at 300 K is multiplied by a factor of 10 (100) for wires (films) for better visibility.

Downloaded 14 May 2011 to 129.74.159.82. Redistribution subject to AIP license or copyright; see http://jap.aip.org/about/rights_and_permissions

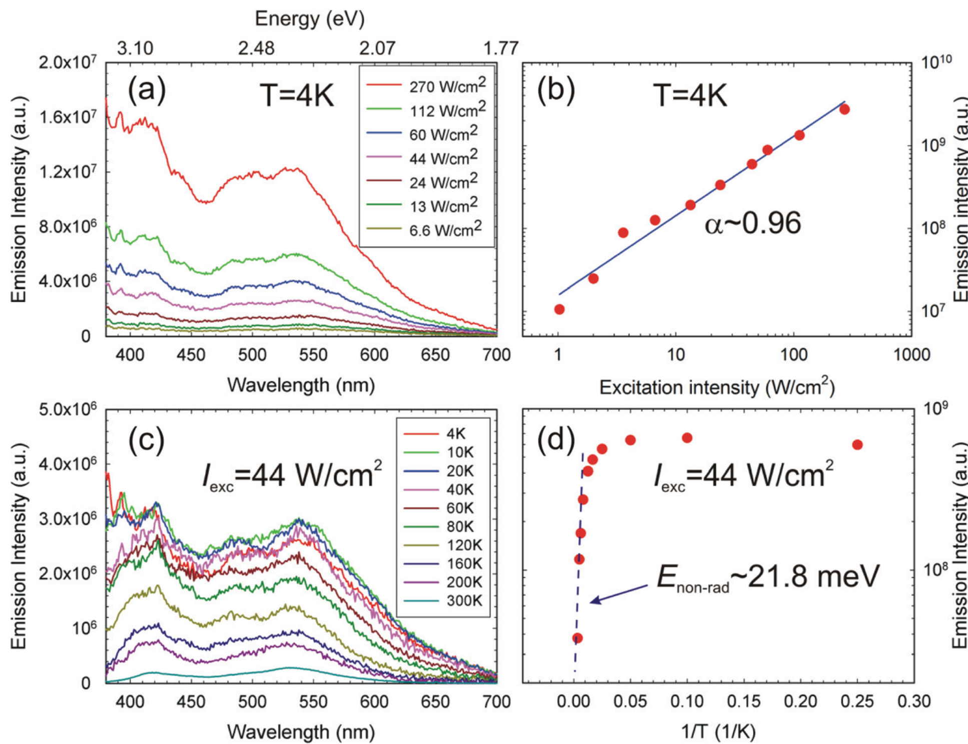

FIG. 7. (Color online) Emission spectra of InGaN wire ensembles measured at various excitation powers at 4 K (a) and temperatures at ∼40 W/cm^2 (c). Right panels exhibit integral emission intensity as function of excitation power (b) and temperature (d).

on the above observations, the room temperature ∼10% QY of the InGaN wires should be ∼50 times higher than that of films having the same ∼20% indium composition. As a side note, it was verified that the small ripples visible in the thin film spectra at 4K [Fig. 6(b)] originate from the Fabry–Perot interference of the emission reflecting between the InGaN/air and GaN/sapphire interfaces. In a control experiment, the InGaN film was grown on a freestanding GaN and the ripples disappeared.

At first glance, the difference in the emission intensities may be attributed to better extraction efficiency for wires vs films. However, more careful analysis indicates that this not the case. With the assumption of isotropic emission from ensembles of as grown wires, the objective with a numerical aperture NA = 0.32 collects ∼1/38 fraction of the total light emitted by the wires. On the other hand, for a smooth semiconductor/air interface, the collection efficiency will be determined by the exiting light cone angle; AFM scans of InGaN films show that they have a rms roughness of ∼3 nm on a 1 μm^2 lateral scale and the film can be considered flat from an optical point of view. Linear extrapolation for n ∼ 2.5 refraction index of $In_{0.2}Ga_{0.8}N$ material[21] yields the exiting cone angle $\alpha = \arcsin(NA/n) \sim 7.35°$. This translates into $2\pi(1 - \cos 7.35°)/4\pi \sim 1/240$ fraction of the total emission traveling toward the objective from the inside of the InGaN thin film. The major part of the light will be trapped inside the film. Therefore, if the difference in the emission intensities is only due to the extraction efficiency, it should be expected that ∼10 times less light is collected from smooth InGaN films compared with wires. In contrast, almost three orders difference in the intensities was detected in the experiments. The data indicates that, probably, the QY of the films is not approaching 100% even at 4 K and that at low temperatures the wires have ∼1–2 orders higher quantum yield. Combined with ∼10 times better extraction efficiency it results in extremely bright emission from InGaN nanowires compared to thin films.

More comprehensive PL data for InGaN nanowire ensembles grown without using GaN seeds and acquired at various temperatures/excitation powers are shown in Fig. 7. The PL spectrum of the nanowires is broad and spreads from a 360 nm GaN peak continuously to a red 600–700 nm colors [for better visibility of the InGaN emission, the GaN peak is not shown in the Figs. 7(a) and 7(c)]. The emission intensity dependence upon the temperature is explained by the exciton dynamics [see the sketch of InGaN band diagram in Fig. 8(d)]. At sample temperatures below 10–20 K the excitons localize in 1–2 meV high potential wells and carrier localization results in the PL spectra "freeze" out. At elevated temperatures, the excitons leave the local potentials and diffuse, sampling larger volumes that contain nonradiative centers. The exponential decay of the emission intensity at T > 20 K is usually ascribed to the emission quenching by nonradiative centers having few tens of meV activation energy E_{nonrad}; the corresponding expression for PL intensity is $I_{PL}(T) = I_{PL}(0)\left(k_{rad}/k_{rad} + Ae^{-E_{nonrad}/kT}\right)$. In this expression, k_{rad} is the exciton radiative rate and $Ae^{-E_{nonrad}/kT}$ defines the temperature dependent nonradiative recombination of excitons. The InGaN wire ensembles presented in this paper exhibit $E_{nonrad} = 35$ meV activation barrier (standard deviation $\sigma \sim 19$ meV), while for films this value is $E_{nonrad} = 29$ meV ($\sigma \sim 5.7$ meV). The larger activation energy E_{nonrad} and broader σ measured for the nanowires reflect higher compositional fluctuations than thin films, which correlates well with a broader spectrum of wire ensembles.

Nonradiative centers can be accessed not only by thermalization of excitons at high temperatures, but also by filling higher energy states at higher excitation powers (the

Downloaded 14 May 2011 to 129.74.159.82. Redistribution subject to AIP license or copyright; see http://jap.aip.org/about/rights_and_permissions

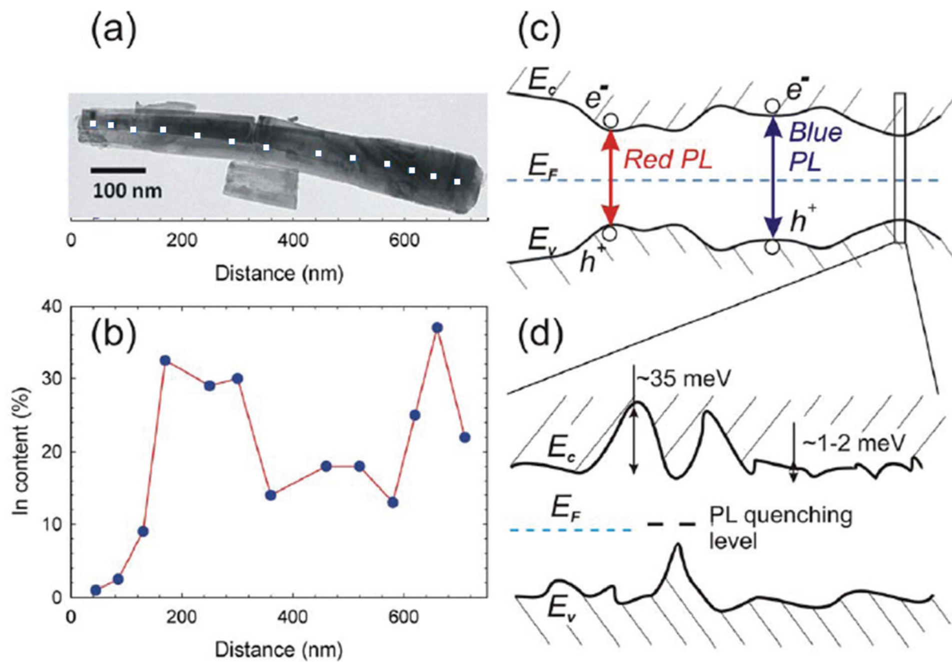

FIG. 8. (Color online) (a) Transmission electron microscope image showing an InGaN wire together with energy-dispersive x-ray spectrometry dwell points. indium content was calculated for each point and the indium microscopic distribution is shown in (b). Nonuniform indium content causes bandgap fluctuations on the microscopic scale as shown schematically in (c) as well as on much finer distances (assumed from photoluminescence) (d).

band filling effect). The following observation was made: in a linear regime, where the emission intensity is proportional to the excitation power, the emission peak did not shift in wavelength. Upon transition to a sublinear dependence at high excitation, a blueshift of the emission peak was observed. This trend is very obvious in single wire PL measurements [Fig. 9(e), for example] or on nanowire ensembles with a narrower emission spectra.

Based on these observations, a qualitative model for the excitation power dependent emission emerges. Efficient radiative recombination occurs near higher In-content inclusions randomly distributed in a wire. Inclusions provide localized states for excitons, which can be characterized by a finite rate of radiative recombination from the lowest energy levels. In a linear regime (at small excitation intensities) the absorption rate is smaller than the radiative recombination rate summed all over In inclusions. Therefore, under low excitation conditions, the emission originates from the lowest levels and its intensity is proportional to the excitation power. Since the excitons recombine from the same levels the emission peak does not shift. At higher excitation intensities the carrier photogeneration rate exceeds the rate of radiative recombination from the lowest levels and the population of higher energy levels increases. This results in a blueshift of the emission peak. In addition, at higher energy levels the radiative rate decreases due to (a) lower overlap of electron and hole wave functions (smaller carrier confinement at extended levels) and (b) smaller E_{nonrad} activation barrier for nonradiative recombination seen by higher energy excitons. It results in a sublinear emission intensity dependence on excitation power.

IV. EDX COMPOSITIONAL STUDIES

The broad emission of InGaN nanowire ensembles ranging from the GaN peak to red colors unambiguously predicts compositional variations in the nanowires. STEM imaging along with EDX spectrometry of the wires was carried out to examine their compositional makeup. EDX spectrometry was performed on various nanowires; grown by nonseeded growth to remove the chance of the seeding being the cause of the indium variation; and at various points along individual nanowire axis on wires harvested on to copper grids using a collection time of two minutes/spot. A quantitative analysis was performed using the Cliff–Lorimer method comparing In(L) and Ga(K) peaks to a standard of known composition.[22] The EDX analysis indicates wire-to-wire indium concentration variations for nanowires harvested from the same growth sample. In addition, the indium concentration along the growth c-axis is nonuniform within individual wires. Similar studies carried out on lamellae composed of nanowires still standing on the growth substrate show similar results. Figure 8 shows a TEM image of a representative wire upon which the EDX beam positions are indicated. The indium concentration along the representative wire varies from 1 to ∼35%. A plot of the indium concentration along the wire shows the variations in the Ga:In ratio along the growth axis. A schematic energy band diagram shown in Fig. 8(c) explains the observed broad PL emission spectrum from the wires. This band diagram was constructed using a bowing parameter of 2.6 eV (Ref. 19) combined with the indium concentration data from Fig. 8(b). Using this bowing parameter, indium concentrations of 35, 22, and 12%, respectively, yield red, green, and blue colors. As seen, emission covering the entire visible spectra is provided from a single nanowire. Figure 8(d) is not based on the EDX data, but is an approximation based on PL measurements. Indium clustering as seen here is not limited to these results. Such indium concentration fluctuations along the growth axis of nanowires are not limited to the III-V nitrides; it has been observed in MBE grown InGaAs nanowires.[23] Additionally, there have been corroborating reports on varying indium

Downloaded 14 May 2011 to 129.74.159.82. Redistribution subject to AIP license or copyright; see http://jap.aip.org/about/rights_and_permissions

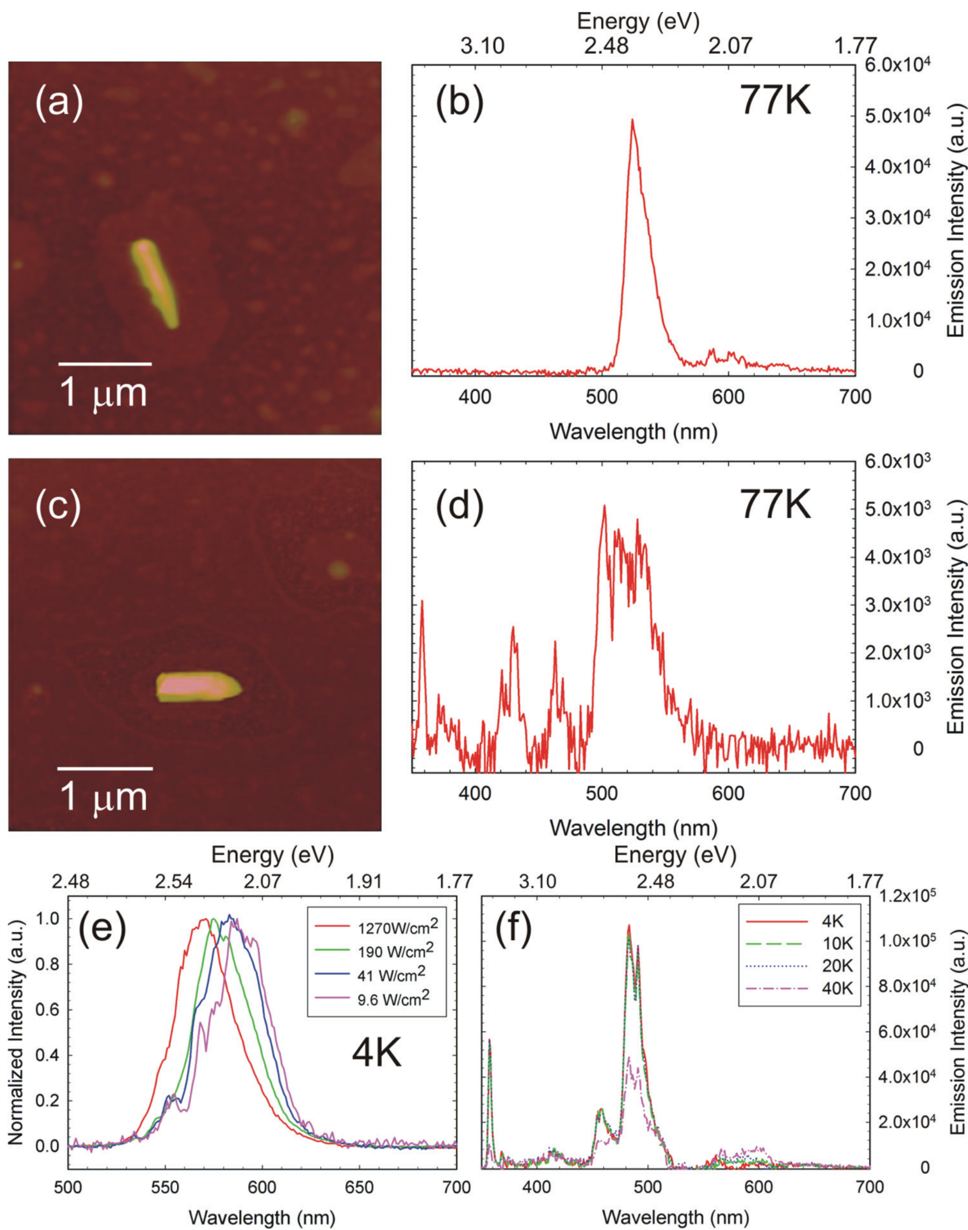

FIG. 9. (Color online) On the left panels (a) and (c) atomic force microscopy images of two single wires are presented. Top (bottom) wire has 30 nm (79 nm) radius. Right panels (b) and (d) exhibit corresponding emission spectra. (e) and (f) represent power and temperature trends measured on two other single wires.

concentrations within 7 nm thick InGaN quantum dots grown in GaN nanowires[24] showing that such behavior cuts across nanostructure shapes as well as semiconductor material systems.

It should be noted that there have been reports of TEM beam damage being the cause of such indium clustering by groups including Smeeton *et al*.[25] They find that the heat generated by a 200 kV beam is well below the required amount to cause phase separation as reported by Ho *et al*.[26] However, according to Ho *et al.*, at a 650 °C growth temperature, spinodal decomposition is likely to occur in InGaN materials. It has also been shown by energy filtered transmission electron microscopy[27] that indium clustering occurs without the use of high beam energies. In this work, there are two notable characteristics relevant to this issue. First, broad PL spectra were acquired from InGaN wires not exposed to high-energy electron radiation, clearly indicating that indium fluctuations are not related to the electron beam exposure. Second, while taking the EDX scans the ratios of the In:Ga peaks remained similar over multiple scans.

Very recent reports on the growth of InGaN wells in GaN nanowires[28,29] suggest that the indium concentration in InGaN nanowires depends on the nanowire diameter along with the spacing between the nanowires due to a shadowing effect. As these wires presented here have a range of diameter (50–100 nm) along with varied spacing, it is possible these two factors influenced the indium concentration in the wires as they grew.

V. SINGLE WIRE PL

Since EDX measurements showed wire-to-wire indium concentration variations, single nanowire PL data was collected to establish the link between experiments. For single

Downloaded 14 May 2011 to 129.74.159.82. Redistribution subject to AIP license or copyright; see http://jap.aip.org/about/rights_and_permissions

wire PL experiments the wires were harvested from the silicon substrate by sonication, and were deposited from an isopropanol solution onto Au patterned quartz cover slips. The Au patterned quartz cover slips were made by optical lithography, which included photoresist deposition, exposure to UV light and wet etching in developer, Ti/Au 5/200 nm thick metal deposition for reference marks, and subsequent lift-off of the remaining photoresist with acetone. The patterned substrate enables precise navigation of the optical path to single wires required in conjoint optical/atomic force microscopy experiments. An atomic force microscope nanoscope V was utilized for locating the nanowires. Vertical and lateral calibration of the microscope was performed on a commercial calibration sample with 100 nm deep grooves separated by 3 μm period.

Single wire experiments revealed that, while the individual nanowire PL spectra depend on the excitation power and temperature the same way that nanowire ensembles do, the wire-to-wire emission intensity and spectra vary significantly. Originally it was expected that, since the wires were harvested from the same MBE sample, they should exhibit similar spectra. This turns to be not the case. Left panels (a) and (c) of Fig. 9 show the AFM images of two individual InGaN nanowire groups that coalesced during growth. The spectra obtained from these wires are quite different. The spectrum in Fig. 9(b) has one well-defined peak in contrast with multiple peaks of the spectrum measured for the thicker wire [Fig. 9(d)]. Figures 9(b) and 9(d) vividly demonstrate the influence of single wire indium content fluctuations on the PL spectra.

The emission spectra of single wires are found to be narrower than of wire ensembles, and therefore are better suited for power and temperature-dependent measurements. Figures 9(e) and 9(f) show the PL spectra measured on two separate single wires at various excitation powers (e) and temperatures (f). The integrated emission intensity for a wire (e) as a function of the excitation power is sublinear ($I_{PL} \sim I_{exc}^{0.76}$) and it correlates with the blueshift of the emission peak at higher intensities (to highlight the peak shift, the emission intensity was normalized to unity). Similar to wire ensembles, the PL spectrum for a single wire (f) does not change for $T < 20$ K. We assigned this effect to the localization of excitons in a few meV deep potential wells caused by local variations of indium composition, as indicated in Fig. 8(d).

VI. SINGLE WIRE QUANTUM YIELD

Precise AFM sizing of individual wires allowed an approximate evaluation of their photoluminescence quantum yields based on comparison of emission and absorption rates. To achieve this evaluation, two obstacles have been overcome. The first obstacle is that the PL spectrum of wires is broad and often exhibits multiple peaks. Under such circumstances, direct applicability of single photon counting devices such as avalanche photodiodes or photomultiplier tubes for emission rate measurements is questionable since the sensitivity of photodetectors and reflection/transmission of optical elements may vary substantially over the broad spectral range of nanowires. Instead, the emission spectra was analyzed and corrected for the objective's collection efficiency, the reflection of gratings, and the PMT sensitivity. After calibrations had been performed, the procedure was tested on $\sim$8.9 μW green light source. The application of the procedure yielded $\sim$5.6 μW source power and factor $8.9/5.6 \sim 1.6$ was included into the emission rate (emitted photons/sec) calculations.

For quantum yield estimates, the rate of absorbed photons needs to be calculated and this depends on both the wire absorption cross-section and the laser excitation intensity. While the excitation intensity can be easily approximated as $\sim$ (excitation power)/(excitation area), the absorption cross-section calculations cause certain difficulties. To overcome this problem, the model for absorption of a long dielectric cylinder embedded into monochromatic electromagnetic wave was applied.[30] (Supporting information of Ref. 30 provides the codes for calculations.) The model was tested on single wire excitation anisotropy[30] and considers heating of nanowires caused by light absorption and has demonstrated a good fit to experimental data.[31] In the model, the only parameter which is material dependent is the InGaN dielectric constant at the excitation wavelength.

In spite of the fact that InGaN alloys are widely used in the manufacturing of blue, UV, and near-UV diodes and lasers, little is known about its optical constants above the bandgap. As a first approximation, a linear fit between dielectric constants of InN and GaN measured or theoretically calculated at 325 nm was used. An averaging of dielectric constants available for both c- and h- phases of GaN (Refs. 25, 32–35) and InN (Refs. 25, 36, 37) semiconductors is employed in order to estimate ε_{InGaN} at 325 nm excitation. Such averaging for (In,Ga)N materials and subsequent linear extrapolation for dielectric constant of $In_{0.2}Ga_{0.8}N$ yields

$$\varepsilon_{InN}(325\text{nm}) = 6.55(\sigma = 0.70) + i2.87(\sigma = 0.67), \quad (1)$$

$$\varepsilon_{GaN}(325\text{nm}) = 6.64(\sigma = 0.25) + i1.73(\sigma s = 0.25), \quad (2)$$

and

$$\varepsilon_{In_{0.2}Ga_{0.8}N}(325\text{nm}) = 6.62(\sigma = 0.24) + i1.96(\sigma = 0.24). \quad (3)$$

The dielectric constant of (In,Ga)N semiconductors strongly depends on the film quality, and corrections for film roughness are necessary.[32] Without such corrections, significant "spread" in numbers appears and it is reflected in the formula (3) by standard deviation for real and imaginary parts of the dielectric constant. Therefore, each wire radius was sampled for all possible combinations between real and imaginary parts in order to get maximum and minimum values for an absorption cross-section. In Fig. 10, the maximum and minimum values are depicted by dots (diamonds).

The absorption coefficient of InGaN nanowires depends on the dielectric constant of a surrounding environment through the boundary conditions for electromagnetic wave on a wire/medium interface. Figure 10 shows the absorption cross-section of a 1 μm long wire excited with a circular polarized light as a function of the wire radius. The two

Downloaded 14 May 2011 to 129.74.159.82. Redistribution subject to AIP license or copyright; see http://jap.aip.org/about/rights_and_permissions

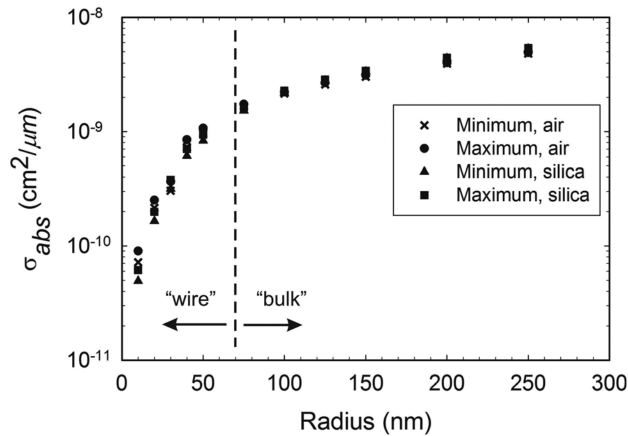

FIG. 10. Triangles (squares) represent the minimum (maximum) of the absorption cross-section of 1 μm long $In_{0.2}Ga_{0.8}N$ wire embedded into fused silica as a function of wire diameter. Minimum (maximum) for wire in air are noted by cross (circle). Vertical dashed line indicates from wirelike to bulklike absorption.

curves reflect the hypothetical scenario where the wire is suspended in air [$\varepsilon_{air} = 1$, (X and circle)] or completely embedded into a quartz dielectric [$\varepsilon_{quartz} = 2.19$,[38] (triangle and square)]. The actual value of the absorption cross-section for individual InGaN nanowires dispersed on quartz slips lies between these two extremes, since the wires reside on an air/quartz interface. The QY was calculated for both of these limits.

Figure 10 also shows that the transition from nanowire-like to filmlike absorption occurs at a wire radius $\sim$70 nm. Below this transition, the absorption grows as $\sim R^{1.7}$, while above it scales almost linearly with the wire radius R. For bulk InGaN, the 325 nm excitation light penetrates approximately $\sim\lambda/4\pi k$ deep into the material [$I_{excitation}(r) = I(0)e^{-(4\pi k/\lambda)r}$, k is the imaginary part of wire refractive index and $\lambda = 325$ nm). When the wire radius R exceeds a light penetration depth, a significant portion of the nanowire volume becomes ineffective in absorbing photons. From Eq. (3), the complex refraction index for $In_{0.2}Ga_{0.8}N$ is $n = 2.6 + i0.38$, and $k = 0.38$ translates into $\sim$70 nm penetration depth for 325 nm light. $\lambda/4\pi k$ $\sim$70 nm determines the transition from wires to films from an absorption point of view and it is reflected in Fig. 10 as a "knee" point where the graph slope changes.

For QY estimates, the wires that contain relatively uniform distribution of In along the growth axis were chosen. Such wires should provide high intensity single peak emission at green wavelengths; the wire in Figs. 9(a), 9(b) fit this criteria, and was chosen for single wire QY analysis. The emission spectrum from this wire shown in Fig. 9(b) peaked in green, and was acquired at an excitation intensity of 22 W/cm^2. Estimates for the emission rate yielded $\sim 7.4 \times 10^9$ photon/s at 4 K. The absorption cross-section for the 30 nm radius, 1 μm long wire excited by 325 nm light falls in the range 3.0–3.8×10^{-9} cm^2 (the limits arise due to uncertainties in dielectric constant of the InGaN material and a surrounding medium). The ratio (excitation intensity $\times$ absorption cross-section)/(photon energy) for the absorption rate yields 1.1–1.4×10^{10} photon/s which translates into 52–67% PL QY, a high efficiency. Clearly, the nanowire surface does not quench the emission. A possibility is that photogenerated excitons become trapped on In inclusions and recombine radiatively before they reach the wire surface.

To explore how the PL spectra of nanowire ensembles evolve from those of single InGaN nanowires, the individual spectra of six single wires from a single growth were acquired and added together (Fig. 11). Each spectrum is from a single wire (a), but their sum clearly resembles the ensemble spectrum (b); on both spectra the GaN peak and peak at 440 nm are visible. For single wire PL measurements the wires which exhibit other than GaN emission peaks were specifically chosen. Single wire PL measurements revealed that there were a significant proportion of wires which exhibit mostly GaN emission. The wires with only GaN emission have been omitted from these measurements. Such a selection for InGaN ensembles was not able to be made, and therefore the emission from low In-content wires is added in the PL spectra of ensembles. This explains the difference in relative intensities of the 440 nm peak in Fig. 11(b).

VII. CONCLUSION

To summarize: (a) Intrinsic inhomogenity in single InGaN nanowire emission spectra caused by compositional fluctuations of the indium content within the wire was observed. (b) The ratio of emission-to-absorption rates for bright single emission peak wires yields a *single wire* emission quantum yield exceeding 50% at 4 K and more than 1% at 300 K; there is insignificant emission quenching caused

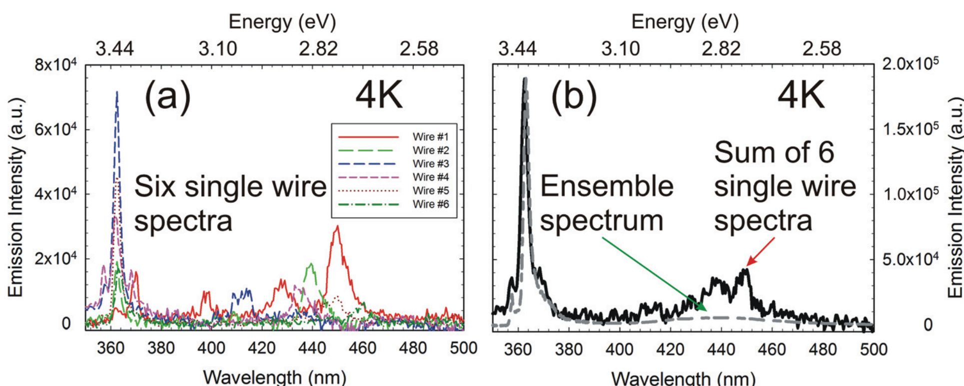

FIG. 11. (Color online) (a) Individual spectra of six single InGaN wires and (b) their sum. For a comparison, the dashed line in figure (b) represents the spectra measured on an ensemble of wires; the GaN emission was normalized to the same value.

Downloaded 14 May 2011 to 129.74.159.82. Redistribution subject to AIP license or copyright; see http://jap.aip.org/about/rights_and_permissions

by the nanowire surface at low temperatures. (c) The PL spectra of single wires as well as ensembles of wires "freeze" below ~20 K due to exciton localization at potential minima. (d) As the excitation intensity increases to hundreds of W/cm^2 the emission peak starts shifting to higher energies due to band filling phenomenon. (e) At low excitations powers (0.1 W/cm^2 < I_{exc} < 100 W/cm^2) PL intensity increases linearly with the excitation power; whereas at higher intensities (up to ~1.5 kW/cm^2) the dependence changes to sublinear, reflecting the process of delocalization of excitons and their successive nonradiative recombination at quenching centers.

On the growth side, using the appropriate substrate temperature InGaN nanowires have been successfully grown by MBE for the first time with PL spectra centered at green wavelengths. Structural analysis showed high quality InGaN material with no defects visible. While the original intent was to grow InGaN nanowires with constant indium content throughout the entire nanowire, the broad emission spectra and complimentary EDX measurements demonstrated that the indium concentrations in the nanowires varied from zero to near 35% along the lengths of the growth axis. This grading occurred in spite of the fact that growth conditions were held constant during the nanowire growths. Additionally, the indium concentration varied from wire-to-wire for wires from the same growth sample. While some wire growths do not offer a sharp emission peak at green wavelengths, their broad spectrum could prove useful in lighting applications such as broad spectrum emitters or phosphors directly integrated on UV or blue LED structures in a single growth step to offer a high efficiency and high rendering index light.

ACKNOWLEDGMENTS

The authors are thankful for the financial support of NSF award Nos. 0645698 and 0907583 monitored by Dr. LaVerne Hess.

[1]A. Zukauskas, M. S. Shur, and R. Gaska, *Introduction to Solid State Lighting* (Wiley, New York, 2002).
[2]T. Detchprohm, M. Zhu, W. Zhao, Y. Wang, Y. Li, Y. Xia, and C. Wetzel, Compound Semicond. **15**, 21 (2009).
[3]K. A. Bertness, N. A. Sanford, and A. V. Davydov, J. Def. Softw. Eng. **19**, 9 (2006).
[4]T. Kuykendall, P. Ulrich, S. Aloni, and P. Yang, Nat. Mater. **6**, 951 (2007).
[5]K. A. Bertness, N. A. Sanford, J. M. Barker, J. B. Schlager, A. Roshko, A. V. Davydov, and I. Levin, J. Electron. Mater. **35**(4), 576 (2006).
[6]C. Calarco, R. J. Meijers, R. K. Debnath, T. Stoica, E. Sutter, and H. Luth, Nano Lett. **5**(5), 981 (2005).
[7]E. Calleja, J. Ristic, S. Fernandez-Garrido, L. Cerutti, M. A. Sanchez-Garcia, J. Grandal, A. Trampert, U. Jahn, G. Sanchez, A. Griol, and B. Sanchez, Phys. Status Solidi B **244**(8), 2816 (2007).
[8]R. K. Debnath, R. Meijers, T. Richter, T. Stoica, R. Calarco, and H. Luth, Appl. Phys. Lett. **90**, 123117 (2007).
[9]Y. S. Park, S. Lee, J. Oh, C. Park, and T. Kang, J. Cryst. Growth **282**, 313 (2005).
[10]L. H. Robins, K. A. Bertness, J. M. Barker, N. A. Sanford, and J. B. Schlager, J. Appl. Phys. **101**, 113505 (2007).
[11]R. Songmuang, O. Landre, and B. Daudin, Appl. Phys. Lett. **91**, 251902 (2007).
[12]A. Cavallini, L. Polenta, M. Rossi, T. Richter, M. Marso, R. Meijers, R. Calarco, and H. Luth, Nano Lett. **6**(7), 1548 (2006).
[13]S. Ishizawa, H. Sekiguchi, A. Kikuchi, and K. Kishino, Phys. Stat. Solidi B **244**(6), 1815 (2007).
[14]K. M. Wu, Y. Pan, and C. Liu, Appl. Surf. Sci. **255**, 6705 (2009).
[15]S. H. Oh, K. van Benthem, S. I. Molina, A. Y. Borisevich, W. Luo, P. Werner, N. D. Zakharov, D. Kumar, S. T. Pantelides, and S. J. Pennycook, Nano Lett. **8**(4), 1016 (2008).
[16]A. Kikuchi, M. Kawai, M. Tada, and K. Kishino, Jpn. J. Appl. Phys. **43**(12A), L1524 (2004).
[17]K. Goodman, K. Wang, X. Luo, J. Simon, T. Kosel, and D. Jena, Mater. Res. Soc. Symp. Proc. **1080**, 1080-O08-04 (2008).
[18]K. A. Bertness, A. Roshko, N. A. Sanford, J. M. Barker, and A. V. Davydov, J. Cryst. Growth **287**, 522 (2006).
[19]M. D. McCluskey, C. G. Van de Walle, L. T. Romano, B. S. Krusor, and N. M. Johnson, J. Appl. Phys. **93**(7), 4340 (2003).
[20]R. Meijers, T. Richter, R. Calarco, T. Stoica, H. P. Bochem, M. Marso, and H. Luth, J. Cryst. Growth **289**, 381 (2006).
[21]A. B. Djurišić and E. H. Li, J. Appl. Phys. **85**, 2848 (1999).
[22]B. Fultz and J. Howe, *Transmission Electron Microscopy and Diffractometry of Materials*, 3rd ed. (Springer, New York, 2008), p. 208.
[23]F Jabeen, S. Rubini, and F. Martelli, Microelectron. J. **40**, 442 (2009).
[24]Y. Chang, J. Wang, F. Li, and Z. Mi, Appl. Phys. Lett. **96**, 13106 (2010).
[25]T. M. Smeeton, C. J. Humphreys, J. S. Barnard, and M. J. Kappers, J. Mater. Sci. **41**, 2729 (2006).
[26]I. Ho and G. B. Stringfellow, Appl. Phys. Lett. **69**(18), 2701 (1996).
[27]H. K. Cho, J. Y. Lee, C. S. Kim, G. M. Yang, N. Sharma, and C. Humphreys, J. Cryst. Growth **231**, 466 (2001).
[28]R. Armitage and K. Tsubaki, Nanotechnolgy **21**, 195202 (2010).
[29]H. Sekiguchi, K. Kishino, and A. Kikuchi, Appl. Phys. Lett. **96**, 231104 (2010).
[30]J. Giblin, V. Protasenko, and M. Kuno, ACS Nano **3**, 1979 (2009).
[31]J. Giblin, M. Syed, M. T. Banning, M. Kuno, and G. Hartland, ACS Nano **4**, 358 (2010).
[32]T. Kawashima, H. Yoshikawa, S. Adachia, S. Fuke, and K. Ohtsuka, J. Appl. Phys. **82**, 3528 (1997).
[33]R. Goldhahn, J. Scheiner, S. Shokhovets, T. Frey, U. Köhler, D. J. As, and K. Lischka, Appl. Phys. Lett. **76**, 291 (2000).
[34]G. Yu, G. Wang, H. Ishikawa, M. Umeno, T. Soga, T. Egawa, J. Watanabe, and T. Jimbo, Appl. Phys. Lett. **70**, 3209 (1997).
[35]R. Goldhahn, S. Shokhovets, J. Scheiner, G. Gobsch, T. S. Cheng, C. T. Foxon, U. Kaiser, G. D. Kipshidze, and W. Richter, Phys. Status Solidi A **177**, 107 (2000).
[36]R. Goldhahn, Acta Phys. Pol. A **104**, 123 (2003).
[37]H. Jin, G. L. Zhao, and D. Bagayoko, J. Appl. Phys. **101**, 033123 (2007).
[38]I. H. Malitson, J. Opt. Soc. Am. **55**, 1205 (1965).

Downloaded 14 May 2011 to 129.74.159.82. Redistribution subject to AIP license or copyright; see http://jap.aip.org/about/rights_and_permissions